ENVIRONMENTAL RESEARCH
LETTERS

PURPOSE-LED PUBLISHING™

LETTER • OPEN ACCESS

Surge of peatland destruction by an advancing front of artisanal gold mining in Amazonia

To cite this article: Natalie Daichendt *et al* 2025 *Environ. Res. Lett.* **20** 044001

IOP Publishing Environ. Res. Lett. 20 (2025) 044001 https://doi.org/10.1088/1748-9326/adb868

ENVIRONMENTAL RESEARCH
LETTERS

OPEN ACCESS

RECEIVED
22 November 2024

REVISED
12 February 2025

ACCEPTED FOR PUBLICATION
20 February 2025

PUBLISHED
11 March 2025

LETTER

Surge of peatland destruction by an advancing front of artisanal gold mining in Amazonia

Natalie Daichendt[1], John P Janovec[2], Mathias W Tobler[3], Florian Wittmann[1], Edgardo M Latrubesse[4], Adam Hastie[5], Natalia Morandeira[6] and J Ethan Householder[1,*]

[1] Wetland Department, Institute of Geography and Geoecology, Karlsruhe Institute of Technology, Rastatt, Germany
[2] Herbario Forestal UNALM, Facultad de Ciencias Forestales, Universidad Nacional Agraria La Molina, Lima, Peru
[3] San Diego Zoo Wildlife Alliance, Conservation Science and Wildlife Health, Escondido, CA, United States of America
[4] Environmental Sciences Graduate Program-CIAMB, Federal University of Goiás, Goiânia, Brazil
[5] Department of Botany, Physical Geography and Geoecology, Charles University, Facultuy of Science, Prague, Czech Republic
[6] Instituto de Investigación e Ingeniería Ambiental, Consejo Nacional de Investigaciónes Científicas y Técnicas—Universidad Nacional de General San Martín, Buenos Aires, Argentina
* Author to whom any correspondence should be addressed.

E-mail: john.householder@kit.edu

Keywords: peatland, swamp, aguagal, buritizal, Mauritia, gold mining, remote sensing

Supplementary material for this article is available online

Abstract

Alluvial sediments bordering rivers of the southern Peruvian Amazon are enriched with gold, which has sustained an artisanal gold mining economy within a biodiversity hotspot for the past several decades. While it is clear that sweeping deforestation by miners has resulted in substantial loss of above-ground carbon stocks and increased greenhouse emissions, the region also harbors a sizable below-ground carbon stock in the form of peatlands, and how these have fared against decades of mining expansion is uncertain. Here, we use Landsat's continuous archival record spanning over 35 years to monitor the expansion of gold mining in a major Amazonian peat complex along the alluvial plain of the Madre de Dios River. We detect over 550 ha of peatland surface area that has been lost to gold mining, potentially accounting for between 0.2 and 0.7 Tg of emitted below-ground carbon. Alarmingly, the majority of this loss (55%) has occurred within the past two years. Mining inside peatlands currently accounts for 9% of total mining, but projections suggest a 25% share by 2027 as mining within peatland is accelerating considerably faster than mining in the alluvial plain as a whole. The startling surge of peatland degradation is synchronous with the arrival of an aggressive mining front into the most distal reaches of the alluvial plain where peatlands are most abundant. Already, 63 of 219 peatlands in the alluvial plain show evidence of mining within their borders, putting over 10 000 ha of peatland area and between 3.5 and 14.5 TgC at imminent risk. The rapid proliferation of gold mining inside peatlands appears to be of such scope as to be an existential threat to the entire peatland complex.

1. Introduction

Defined by their organic-rich and wet soils, peatlands are unique environments placed squarely at the forefront of biodiversity loss and climate change (Leifeld and Menichetti 2018, UNEP 2022). As a result of long-term sequestration of atmospheric carbon, peatlands have provided a net cooling effect on global climate for millennia (Yu *et al* 2010, Lähteenoja *et al* 2012, Draper *et al* 2014). As valuable habitat, they sustain and enrich regional biodiversity by providing rare or exclusive resources for flora and fauna (Desrochers and van Duinen 2006, Posa *et al* 2011, Householder *et al* 2015, van der Hoek *et al* 2019). Such attributes offer high benefit/cost opportunities for both biodiversity and climate initiatives, yet even as prioritized ecosystems peatlands and their services continue to be degraded at rapid pace, particularly in tropical regions (Joosten 2010, Page *et al* 2011, Leifeld *et al* 2019, Mishra *et al* 2021).

Amazonia is a major peat-producing region in the tropics, with peatlands covering 128 671–373 359 km^2 according to latest predictions (Hastie *et al* 2024). Although much of this peatland area is expected to be relatively little-disturbed, systematic monitoring of threats is scarce, and most peatlands in Amazonia lack any type of scientific ground verification at all (Lähteenoja *et al* 2012, Roucoux *et al* 2017, Hastie *et al* 2024, Marcus *et al* 2024). Alleged threats include a growing list of predictable culprits, such as agricultural conversion, cattle grazing, fire, fish harvesting, as well as timber and non-timber product extraction, but much of the existing information about peatland degradation in Amazonia still remains anecdotal (Janovec *et al* 2013, Lasso *et al* 2016, Roucoux *et al* 2017). Given the lack of detailed ground information and monitoring, it seems safe to assume that risks to peatlands remain largely undiagnosed throughout much of Amazonia, a regrettable state given that disturbances to peatlands can have disproportionate impacts on carbon stocks, greenhouse emissions, and local ecology (Page *et al* 2002).

Here, we focus on one of Amazonia's major peatland complexes located in Madre de Dios, southern Peru, to address its most pressing threat, artisanal gold mining. Although 'artisanal' refers to the relatively small spatial scale of individual operations, cumulative impacts are considerably larger in scale and harm ecosystem health and services. Artisanal gold mining in the region has been well-documented in recent years, particularly as the underlying regional-to-global economic, political and social drivers that vitalized gold mining in the past, have only increased over time (Swenson *et al* 2011, Asner *et al* 2013, Elmes *et al* 2014, Asner and Tupayachi 2016, Caballero Espejo *et al* 2018, Nicolau *et al* 2019, Dethier *et al* 2023). However, interactions between mining and peatland still remain unassessed.

At risk are approximately 300 km^2 of peatland that have developed near the distal margins of the Madre de Dios alluvial plain (Householder *et al* 2012). Although total peat carbon stocks are still poorly constrained (95% CI = 8.67–36.19 Tg C, mean = 17.64 Tg C), it is relatively clear that due to considerable peat depth, the below-ground carbon density of Madre de Dios peatlands (95% CI = 295–1224 Mg C ha^{-1}, mean = 578 Mg C ha^{-1}) is high relative to other Amazonian peatlands, and up to an order of magnitude higher than above-ground carbon stocks of nearby (non-peat) forests (mean ± sd = 84 ± 36 Mg C ha^{-1}) (Asner *et al* 2010, Draper *et al* 2014, Csillik and Asner 2020, Hastie *et al* 2022). Undoubtedly, more accurate accounting of mining impacts should include peatland loss.

Combining extensive ground experience and historical Landsat imagery, we map out nearly four decades of gold mining disturbances in the alluvial plain of the Madre de Dios river at 30 m spatial resolution and annual temporal resolution. We examine spatio-temporal patterns with particular reference to peatlands, paying particular attention to (i) capturing the long-term spatial and temporal trends of mining in the Madre de Dios alluvial plain, (ii) detailing the expansion of mining activities within peatlands, and (iii) describing the river-to-terrace encroachment of miners into the alluvial plain.

2. Methods

2.1. Madre de Dios peatlands

Madre de Dios peats have a cumulative surface area of 29 400 ha (figure 1), and include among the deepest peats (exceeding 9 m) yet recorded in Amazonia (Householder *et al* 2012). Peatlands are typically located near the margins of the late Quaternary alluvial plain, which is delimited on its northern and southern boundaries by higher, older terraces and tertiary outcrops (figures 1(b) and (c)) (Räsänen *et al* 1992, Rigsby *et al* 2009, Latrubesse *et al* 2010). Upstream of the Inambari river, the alluvial plain consists of lower-intermediate terraces of late Pleistocene deposits, while Holocene deposits formed by the active floodplain and a lower terrace with middle-late Holocene deposits comprise the alluvial plain downstream of the Inambari. Peatlands mostly develop at the distal margins of this alluvial plain where the prevailing hydro-geomorphological site conditions are favorable. Specifically, year-round water logging on these sites is maintained by local rainfall, water table saturation, and seepage from the surrounding uplands, as well impermeable subsurface clay layers (Householder *et al* 2012, Householder and Page 2022). In these peripheral positions, peatlands initiate on flat or poorly drained areas such as those related to backswamps and meander scars. Pollen core profiles indicate that initial plant communities of peatlands are strongly coupled to a more seasonal, riverine flooding regime, including fluctuating water tables, fast sedimentation rates, and low peat accumulation (Wang *et al* 2022). Peat buildup is associated with increasing hydrological and sedimentary isolation from the river, along with a rising dominance of the arborescent palm, *Mauritia flexuosa* (Arecaceae) (Wang *et al* 2023). The palm is widely held to be a keystone species with which a wide spectrum of local biodiversity interacts for food, shelter, refuge, and nesting, and peatland habitat undoubtedly provides unique resources for flora, fauna, and humans (Gilmore *et al* 2013, van der Hoek *et al* 2019). The climate is a lightly seasonal, tropical climate, with average yearly precipitation of 2200–2400 mm, with about 3 months yr^{-1} averaging less than 100 mm.

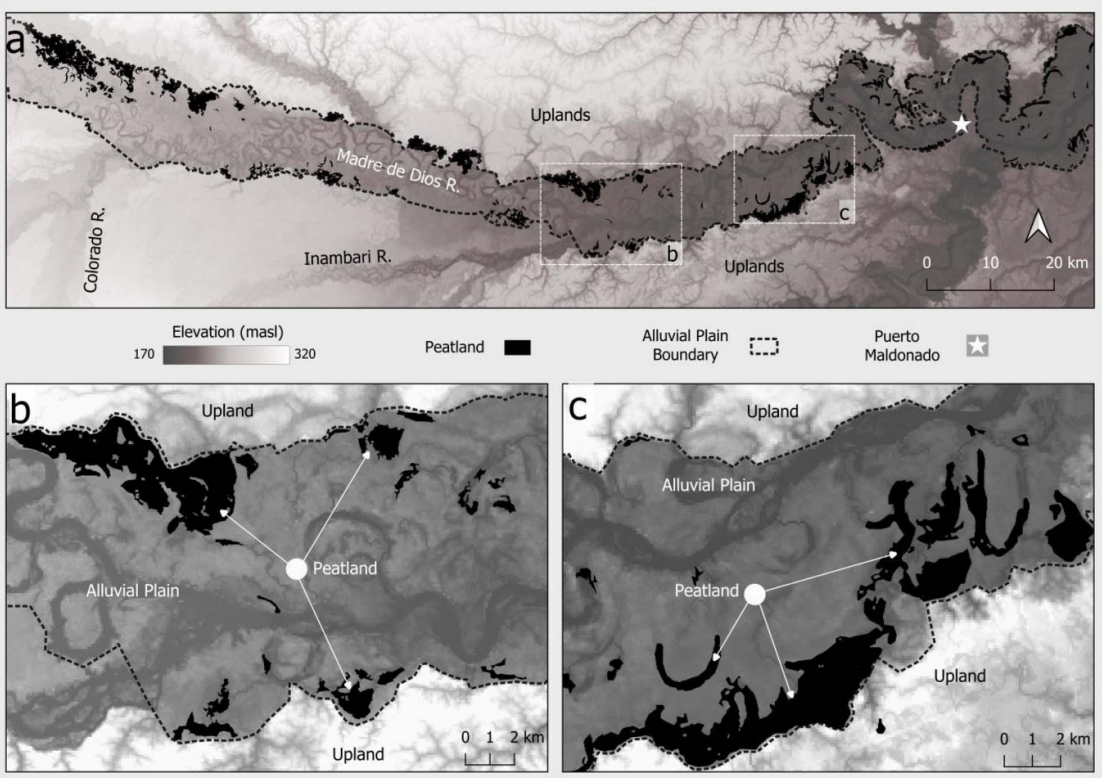

Figure 1. Geographic distribution of peatlands in the Madre de Dios river alluvial plain (a), (b), (c). The alluvial plain under study covers approximately 3000 km^2 along a 250 km^2 stretch of the river, comprising recent floodplain and low-lying terraces of Holocene–Pleistocene origin. This alluvial plain supports a variety of irregularly- to permanently-flooded forests, but peatlands reach their largest extent in low areas of its periphery, often directly abutting older and higher terraces or tertiary rocks. These peripheral sites favor peat buildup because they are hydrologically and sedimentarily disconnected from the currently incised river. Influence from river flooding and river meandering is limited, and local rainfall-water table saturation and ground seepages maintain waterlogged conditions year-round.

2.2. Mining in Madre de Dios

The Madre de Dios region sustains 70% of Peru's artisanal gold production, which is the main source of employment and income for more than 30 000 people—although accurate statistics may be difficult to find given that much of the gold economy is informal (*Kuramoto 2001*, *Salo et al 2016*). Illegal gold mining has been acknowledged since the 1970s and has grown quickly in the weak labor market since the 2000s, particularly following the 2008 global economic recession (Caballero Espejo *et al* 2018). Attempts to formalize mining with clear permitting requirements, property rights, and environmental protections appear to be unsuccessful so far (Salo *et al* 2016, Caballero Espejo *et al* 2018). Gold mining is a principal contributor to deforestation in the region (Asner and Tupayachi 2016, Nicolau *et al* 2019) and is a large source of atmospheric mercury, which bioaccumulates up the food chain and leads to neurological and organ dysfunctions in animals and humans in the region (Yard *et al* 2012, Diringer *et al* 2015).

Individual mines along the Madre de Dios alluvial plain are relatively small in scale (several to several hundred hectares) and employ motorized suction pumps to wash sediments through sluices (Elmes *et al* 2014, Caballero Espejo *et al* 2018). Gold miners use a variety of techniques, not all of which are easily detected through remote sensing products. We have observed dredge boats rigged from two or more canoes that support a platform large enough for a sluice, suction pumps, and small living quarters for a few people. These floating operations scrape alluvium directly from the channel bottom and therefore leave no lasting terrestrial footprint that can be reliably detected through remote sensing. Another common form of mining, also associated with the river channel, involves a single operator using a powerful water hose to blast alluvium from channel edges. Using remote sensing products, this form of mining is difficult to distinguish from natural lateral erosion of the meandering channel. A considerable portion of mining, however, occurs farther inland from the river channel and deeper into the alluvial plain. These operations are associated with rapid removal of forest cover, exposure of bare alluvium, and its replacement with a heterogeneous mix of sand-gravel tailings scattered with water-filled pits. These mined areas offer clear spectral signals for remote detection, are *the* principal threat to peatlands, and our primary focus.

2.3. Remote sensing approach

We identified the timing and location of mined areas using a two-step process (for an illustrated overview see supplementary figure 1). First, we examined the archival Landsat Mission record (since 1985, Landsat 5-TM, 7-ETM+, 8-OLI, and 9-OLI2) for deforestation by identifying drops in Normalized Difference Vegetation Index (NDVI), pixel-by-pixel. Second, we used supervised classifications to discriminate pixels that were deforested by mining, as opposed to other causes. The approach results in a dataset that pinpoints where and when mines appear in the alluvial plain at 30 m pixel spatial resolution and at annual temporal resolution spanning from 1986 to 2023. All remote sensing methods were restricted to a 3104 km^2 area of the alluvial plain that was digitized with the aid of elevation data.

2.3.1. Detecting deforestation

To detect forest losses, for every Landsat pixel we examined the full time series of the NDVI to identify rapid drops consistent with deforestation. To do this we used LandTrendr, a spectral-temporal segmentation algorithm implemented in Google Earth Engine (GEE) that detects changes in temporal trajectories of spectral bands and indices (Kennedy *et al* 2018, Kennedy and Braaten 2020). The principal output is a raster with values for each pixel corresponding to the year of deforestation (i.e. large loss of NDVI) (supplementary figure 1(c)). We implemented LandTrendr using Landsat images from 1985 to 2023, pre-processed with relative radiometric normalization and cloud screening rules to account for multiple Landsat sensors (Kennedy *et al* 2010). LandTrendr parameters were set to detect NDVI losses that were consistent with a rapid replacement of existing forest vegetation with bare substrate by miners (that is, large in magnitude, abrupt, and enduring) (supplementary figure 2). Specifically, the minimum year-to-year loss of NDVI for detection (magnitude) was set to > 0.4, which reflects a major vegetation disturbance (Bao *et al* 2014, Karan *et al* 2016, Dlamini and Xulu 2019). In our preliminary assessments with ground-truthed data, intact floodplain forest had a median NDVI of 0.87, whereas mines had a median NDVI of 0.23. The minimum NDVI value before the change event (preval parameter) was set to > 0.6, to ensure that losses reflect removal of forest, rather than previously disturbed sites. The minimum patch size was set to 3 contiguous pixels, corresponding to approximately a quarter of a hectare (2700 m^2). Losses associated with rapid vegetation recovery (> 0.6 NDVI) within the first three years after the disturbance were not allowed. After mining, forests are slow to recover, so a three-year minimum reduces the chance that seasonal or ephemeral phenomena that may also affect NDVI (deciduous trees and canopy gap formation) are incorrectly captured as deforestation events. We accepted defaults for other parameters. Over the nearly four-decade period it is conceivable that a single pixel experiences numerous rounds of deforestation, mining, regrowth and deforestation. To account for this possibility, we generated two LandTrendr raster outputs for both the year of the first and year of the last deforestation event detected in each pixel time series.

2.3.2. Distinguishing mines

To distinguish deforested pixels associated with mining, as opposed to other phenomena that may also result in deforestation, we generated 11 Maximum Entropy (MaxEnt) predictions spaced at approximately regular intervals throughout the time period (1985–2023). MaxEnt is a probabilistic one-class classifier favorably suited for our purposes because it requires training for only one land cover type (Phillips *et al* 2004, 2006). The MaxEnt predictions were implemented on 11 Landsat median composites (Level 2, Collection 2, Tier 1 surface reflectance, path/row = 02/69 and 03/69) built up from scenes within a one- to two-year time frame, depending on scene quality and cloud cover (Landsat 5 Thematic Mapper (TM) = 1985–1987, 1987–1990, 1996–1998, 2002–2004, 2005–2006, 2007–2008; Landsat 8 (OLI) = 2010, 2013–2014, 2017, 2022, 2023). For each individual composite, we filtered for scenes with less than 30% cloud coverage, and masked cloud and cloud shadow.

Training data for MaxEnt mine predictions was based on over 800 georeferenced points associated with Householder *et al* (2012) (supplementary figure 1). Ground-truthed mining points were used to train the 2010 median composite, which had the closest temporal overlap to the date range of the fieldwork (2008–2010). In unambiguous cases, we also supplemented ground verification points using a combination of high-resolution imagery (visualized through Google Earth) and the Landsat composite to detect mines. Mined areas are spectrally differentiated from surrounding land covers by their heterogeneous mix of gravel, sand, and water, and are therefore readily distinguished in a R-G-B combination displaying the Short Wave Infrared, Infrared, and Red spectral bands. Because ground verification points were restricted to a short time period relative to our entire time span of interest, training for composites at increasingly earlier and later times relied more heavily on spectral patterns of the Landsat composites themselves, combined with high-resolution imagery. For each composite year, we sampled 100–300 mining points, avoiding multiple points in the same individual mine in order to reduce the level of spatial auto-correlation between training and testing sets, which can improperly inflate post-classification accuracy assessments. For each training point we sampled raw spectral information from visible and infrared bands. Background spectral information was sampled from 10 000 random points within

the alluvial plain. To assess the classification, we separated ground points into training (70%) and validation (30%) sets—implementing a spatial join to set a 1 km minimum distance (most mines have a smaller diameter) between testing and validation points to reduce spatial autocorrelation—and computed the area under the curve (AUC) on the validation set (supplementary figure 1(e)). As a probabilistic classifier, threshold values were needed to produce a final binary classification (mined versus not mined). Thresholds were chosen with the aid of the Receiver Operating Characteristic (ROC) to maximize true-positive rates and minimize false-positive rates. Threshold choices, although optimized by the ROC, will inevitably introduce some disagreement in whether a given pixel is identified as mine or not. To examine this level of uncertainty we iteratively (times = 999) allowed thresholds for each MaxEnt classification to vary as a random number with a range 20% higher and lower than our optimal threshold determined by the ROC. Validation was not possible for the two earliest MaxEnt classifications (1985–87 and 1987–90) because unambiguous cases of mining activity were quite rare in the imagery. In these two exceptions, we implemented the classification using spectral information extracted from mined points of the nearest, 1996–98, composite where more spectral information could be obtained, and applied the same threshold to produce the binary classifications.

Preliminary results of the MaxEnt classifications revealed considerable spectral similarity of mines to natural sand bars that form along river edges. As the Madre de Dios River is quite dynamic, we opted to mask out the entire meander band, which included all lateral channel erosion and deposition over the whole time span. For this, we generated yearly river (open water/wetted channel) rasters following Boothroyd *et al* (2021). Briefly, the approach implements cloud masking and a median reducer in the GEE environment to generate a temporal composite within user-defined temporal and spatial window. Multispectral indices, including MNDWI, EVI and NDVI, are then used to classify the composite for the wetted river channel and alluvial deposits. We merged all river outputs for all years to a single mask. This final mask excludes the area directly impacted by the migrating channel, which typically extends a few hundred meters to the current river channel, but in some particularly dynamic areas can broaden to about 1 km. The total masked area accounts for 395 km^2, or 12% of the total region under consideration, and will also undeniably mask out the fraction of mining that may have occurred within. As our main interests lie in understanding how mining interacts with peat, which invariably occurs deeper inside the alluvial plain, the loss is negligible.

All GEE outputs (LandTrendr and MaxEnt) were imported into the R environment (R Core Team 2022), where we implemented spatial and temporal screening. Specifically, all pixels retained from this screening satisfied three conditions: (*i*) they were identified by LandTrendr as deforested, (*ii*) they were identified by the MaxEnt binary classification as mined, and (iii) the discriminating MaxEnt from point *ii* was made from scenes neither prior to, nor long after the year of deforestation detected in point *i*. For this latter time constraint, we required a positive mine identification to originate from at least one of two MaxEnt classifications immediately following the year of deforestation. The resulting dataset, available as a text file (supplementary data 1), pinpoints where and when mines appeared on the landscape at 30 × 30 m spatial resolution and annual temporal resolution.

2.4. Spatial and temporal patterns of mining

Broad-scale geographic patterns were visualized by calculating the cell-wise mined surface area on a 2 km grid. To group individual mine pixels into distinct mine clusters, we used a density estimator, with a 30 m kernel, and polygonized a binary version of the resulting density raster (positive density or not) to delimit the final mine clusters. For all analyses requiring spatial information about peatland, we used the original, unmodified 2012 peatland map of Householder *et al* (2012), itself based on Landsat scenes from 2000–2001. Mining in peatlands appears to be very rare before 2000, as preliminary analyses indicated virtually no consistently detectable mining in peat until several years afterwards. Yearly sums of mined surface area are presented for the entire area under consideration, as well as the subset of mining detected inside peatlands. For each, the observed annual increase in mining was modeled both as an exponential and linear trend (the latter only since 2018, when the trend might be roughly considered as linear), including 5 year extrapolations from 2023.

To develop a geographic model of mine expansion, we examined spatio-temporal trends along the lateral gradient of the alluvial plain (river to terrace). Based on ground experience, we hypothesized that mining has likely been most prevalent in more accessible sites near the main river channel—the principal conduit for all economic activity—and over time expanded to increasingly more remote (river-distant) regions of the alluvial plain. This process describes a heteroskedastic pattern where variation in the distance between mines and river increases over time. To model this pattern, we first generated a river proximity raster, with each pixel value corresponding to its distance to the Madre de Dios river. For each year we iteratively sampled (times = 999) 300 random mine pixels, with replacement, extracted river distance information, and calculated the 20th, 50th, and 80th quantiles, representing the back end, middle, and front end of mining. For each iteration we simultaneously generated 300 random points inside

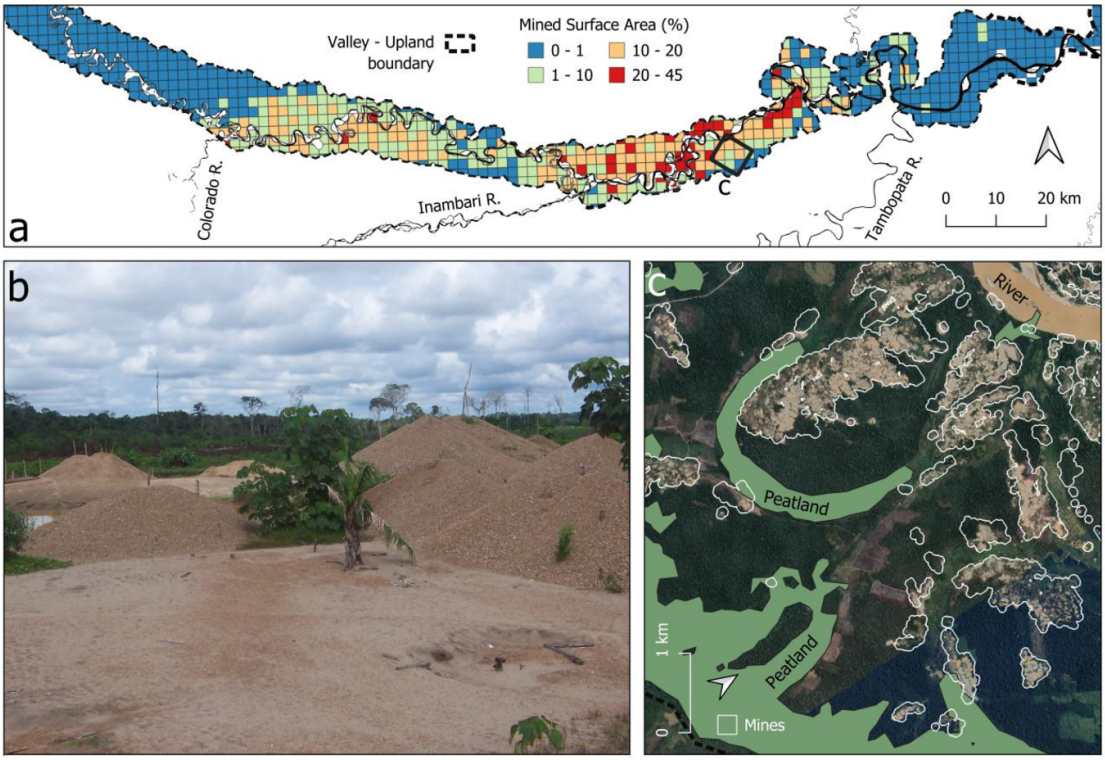

Figure 2. The geography of gold mining in the Madre de Dios alluvial plain. (a) Mines are ubiquitous along approximately 140 km of alluvial plain. Mined surface area is highest along two 40–50 km reaches downstream of the Inambari and Colorado Rivers. The region of the alluvial plain spanning the mouths of the Colorado and Tambopata Rivers includes 98% of mined surface area, and 50% of peatland area. (b, c) Deforested scars resulting from mining activities are plainly visible in high-resolution imagery visualized through Google Earth. Some mine predictions (white outlines) appear to cover unmined forest because the mining is more recent than the date of the high resolution imagery. Photo by J. Ethan Householder. Google Earth 2020—Maxar Technologies/Airbus.

peatlands and calculated the 50th quantile of distance to the river. Thus, information about the landscape positions of both peatlands and mining were sampled with respect to the same river-terrace gradient in a comparative way. As miners move over time, but peatlands do not, we examined mine expansion into the alluvial plain over time using linear regression, and contour modeling to illustrate the typical range of peatlands along the river-terrace gradient.

Analyses were performed using QGIS (v3.34.5) and R statistical software (R Core Team 2022). Data table manipulation was done with the R package *reshape* (Wickham 2007). Spatial data files were read and processed with *terra* (Hijmans 2024) and *raster* (Hijmans 2021). The AUC was carried out using *ROCR* (Sing *et al* 2005), *vcd* (Meyer *et al* 2006), *boot* (Davison and Hinkley 1997, Canty and Ripley 2021) and *pROC* (Robin *et al* 2011).

3. Results and discussion

By all statistical accounts, our supervised classifications identified mines quite successfully—the AUCs for each of the 11 prediction maps were above 0.9 and adjusting the binary thresholds 20% higher or lower from the optimal thresholds introduced little variation in yearly or total mining sums (supplementary tables 1 and 2). Nevertheless, we noticed that our methods predict some mined surfaces better than others. In particular, some open water bodies remained undetected (supplementary figure 3). These ponds can have considerably heterogeneous spectral patterns according to their age and level of mining activity (Dethier *et al* 2023). In addition, their small surface area relative to the Landsat pixel size adds considerable difficulty in accounting for such fine-scale heterogeneity during supervised training. Our predictions of mined surface area are therefore conservative estimates, but as ponds are relatively small and scattered throughout other, more readily recognizable mined surfaces, the spatial and temporal information and analyses that we provide are quite robust to this loss.

3.1. Mining in the alluvial plain

We detected 11 356 ha (95% CI = 11 223–11 489 ha) of mined surface area in the alluvial plain, spanning across an approximately 140 km river stretch located between the mouth of the Colorado River to the west, and the Tambopata River to the east (figure 2). Mining is unequally distributed along the alluvial plain, with approximately two thirds of mined surface area located within a 50 km stretch downstream

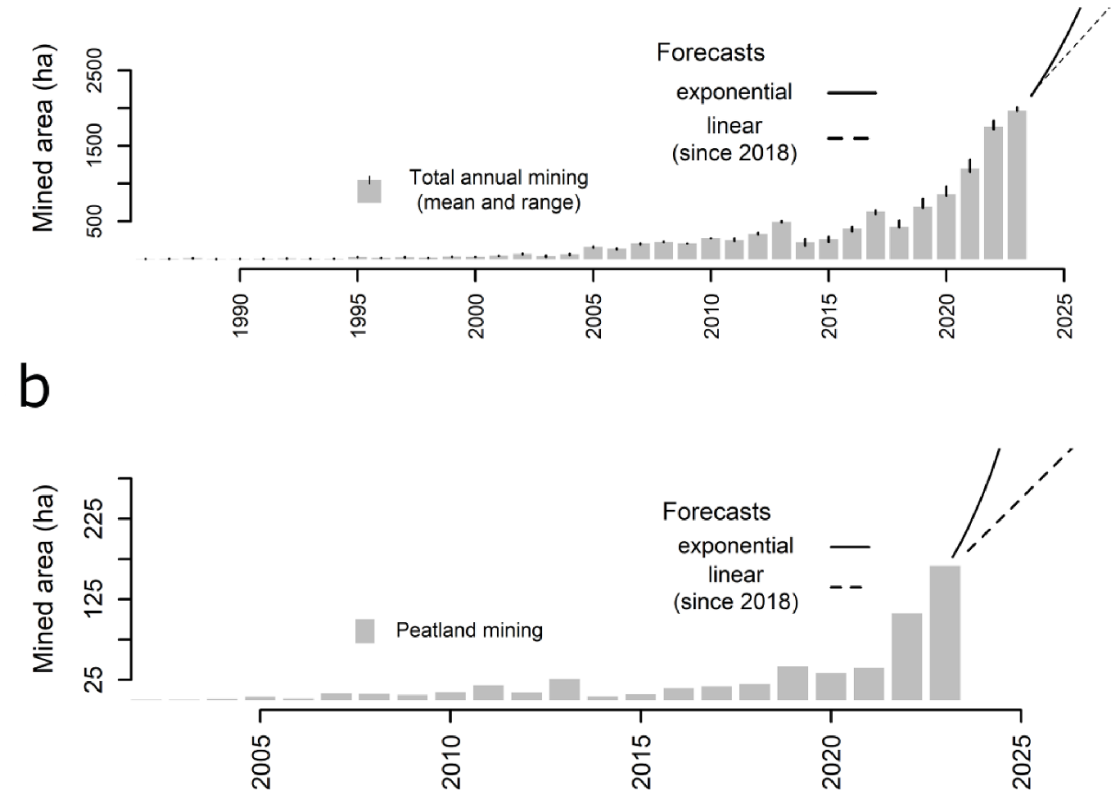

Figure 3. The annual growth of gold mining in the alluvial plain (a) and that of the subset occurring within peatlands (b). Mining inside peatland currently accounts for 9% of all mining in the alluvial plain, but doubles at a rate twice as fast, according to exponential models fit on observed data. Extrapolations of exponential models (solid lines) suggest that mining inside peatland will account for a 25% of total gold mining within five years. Error bars (a) illustrate the maximum and minimum areas obtained after allowing binary MaxEnt thresholds to vary as a random number with a range 20% higher and lower than our optimal threshold determined by the ROC.

from the mouth of the Inambari river. A secondary concentration, accounting for another third of mined area, occurs along a 40 km stretch downstream of the Colorado river. In both hotspots, mines comprise, on average, approximately 12.4% ± 8% (mean ± sd) of the alluvial plain land surface, although this percentage varies substantially from site to site—proportions are double or triple this mean over a cumulative surface area of 18 000 ha.

Individual mines develop as outward spreading patches and coalesce into larger patches over time. The typical mine (median values) has been active for 18 years, initiated in 2004–05, and is 20 ha in size. Twelve mines are over 100 ha in size, these typically initiated in 1997 and active for 26 years (median values). A total of 278 distinct mine patches account for 80% of all mined surface area, and 96% of these mine patches show recent mining activity since 2022 (and all, with a single exception, show activity since 2018). Essentially, all mine patches are active and expanding.

Over time, cumulative mining in the alluvial plain has grown exponentially (figure 3(a)), doubling every 3.3 years according to the fitted non-linear model (supplementary table 3). Model projections indicate that by 2027, over 5000 ha yr^{-1} of forest will be converted to mine (a more conservative linear model indicates over slightly over 3000 ha yr^{-1}), up from the slightly over 2000 ha observed for 2023. Mining has, on average, accounted for 77% of deforestation in the alluvial plain since 2018, up from a mean share of 52% of deforestation in the 2000–2005 time span. For over two decades, therefore, gold mining has been the single largest and fastest-growing source of deforestation in the alluvial plain.

3.2. Mining inside peatlands

We detected over 569 ha of mined peatland surface area, potentially accounting for between 0.2 and 0.7 Tg of below-ground carbon (assuming carbon density estimates of Madre de Dios peatlands from Hastie *et al* 2022). Peatland mining has historically been quite rare, but we detected steady growth since 2000 and most peatland loss (55%) has occurred within the past two years (figure 3(b)). Prior to 2000, peatland mining accounted for less than 1% of the total mined surface area, but by 2023 accounted for a share of 9%. An exponential fit of the time series for peatland mining indicates a 1.5 year doubling time, meaning that the growth rate of gold mining inside peatlands is twice the average for the alluvial plain.

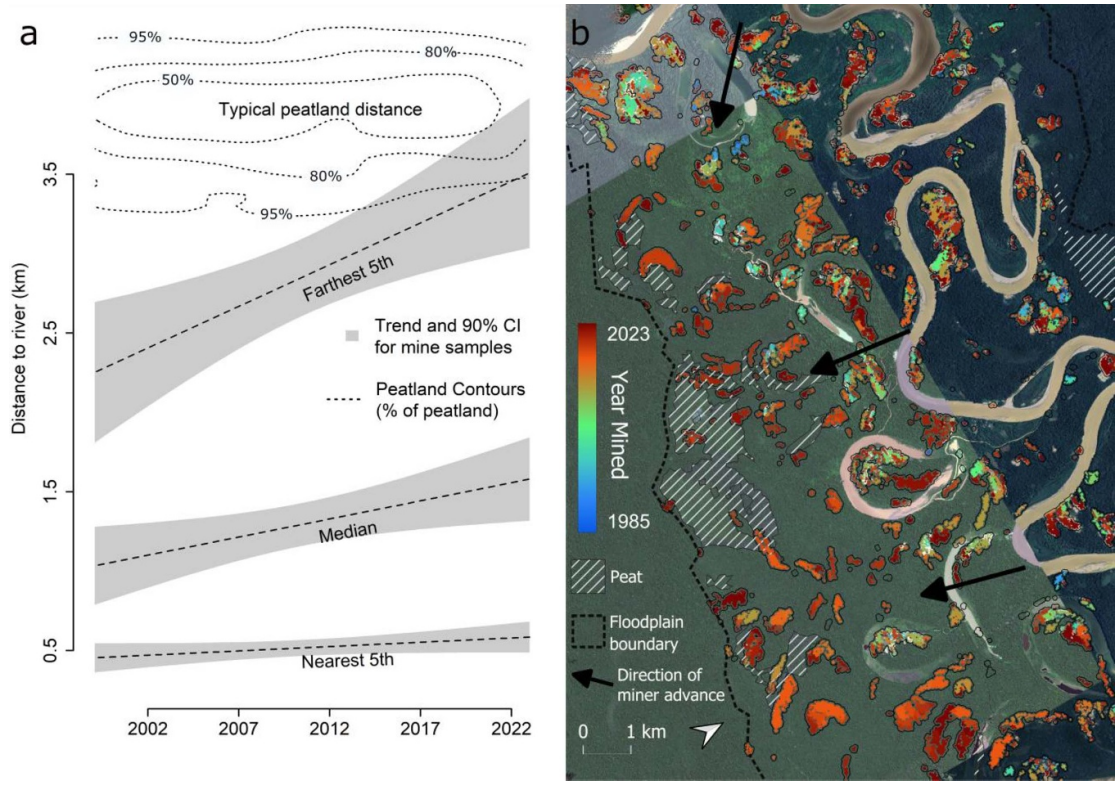

Figure 4. Spatiotemporal patterns of mining in the Madre de Dios alluvial plain. (a) Two decades ago mining activities were confined to a narrow belt less than 2 km from the river channel. Mining near the river channel still continues to be prevalent, as neither the median nor the nearest fifth of mine distances from the river have changed appreciably over the decades. In contrast, the farthest fifth of miner activity has increased considerably, representing an advancing front that has steadily pushed farther from the river and deeper into the alluvial plain at an average rate of 100 m yr^{-1}. This aggressive front has recently reached the periphery of the alluvial plain where peat is most abundant (contours). (b) A 15 km stretch of river illustrating this geographical expansion from the river channel. Near the river channel, mined areas are a mixture of both old and recent, while deeper into the alluvial plain only recently opened mines prevail. Google Earth 2010—Airbus/Maxar Technologies/Landsat/Copernicus.

Within the active mining stretch (between the mouths of the Colorado and Tambopata rivers), the majority of peatlands (60%) show evidence of mining within their borders. Most unaffected peatlands are located farther up- or farther downstream.

Extrapolation of an exponential growth model of peatland mining predicts that by 2027, mining will consume over 1500 ha of peatland annually and account for a 25% share of total mining in the alluvial plain, a three-fold increase of its contribution observed in 2023 (figure 3(b), supplementary table 3). A more conservative linear model (fit only on the last five years of mining data) predicts 400 ha yr^{-1} of converted peatland by 2027. While there is a strong disparity between linear and exponential projections, both are alarming given the fact that the average peatland is merely 200 ha (ranging from 10 to 3500 ha) and 93% of peatlands have a surface area under 400 ha. Although the future uncertainties are large, historical data alone seem evidence enough to make it clearer than ever that mining in the peatland system is both currently ongoing and happening at a scale sufficiently large to threaten the future existence of peatland on the Madre de Dios landscape.

Our spatio-temporal analysis of gold mining along the river-to-terrace gradient offers one possible geographic-oriented hypothesis for the recent surge in peatland mining. We found that historically, much mining has been spatially confined to a rather narrow belt adjacent the river channel. The typical mine in the year 2000, for example, was less than 1 km from the river (figure 4(a), median line). Accessibility may be the most straightforward explanation—as the alluvial plain lacks major roads, the river channel provides the sole access to anywhere. In contrast to the easy access that the river provides, peatland develops more abundantly towards the edges of the alluvial plain—on average between 3.5 and 4.5 km from the river channel—where the hydrogeomorphic context is more favorable for peat accumulation (figure 4(a)—contours). While this peripheral landscape position may have isolated peatland from most mining activity in the past, our results clearly expose an aggressive front of mining that has more rapidly pushed deeper into the alluvial plain at an average rate of about 100 m yr^{-1} (figure 4(a)—farthest fifth). Over time, therefore, the geography of peatlands and the geography of mining have become progressively superimposed. For peatland that was

previously remote and impractical for miners, the forward front of mining has presumably made it increasingly accessible.

4. Conclusion

Madre de Dios peatlands are expected to store 17.64 Tg C (95% CI = 8.67–36.19 Tg C), but on a surface area just 14% the size needed for an equivalent amount stored as forest biomass above ground (carbon density estimates according to Hastie *et al* 2022, Csillik and Asner 2020). By any area-to-area comparison, these peatlands are decidedly carbon-dense and their degradation will have disproportionate impacts on greenhouse emissions. Based on our analyses of the spatial and temporal patterns, it seems reasonable to conclude that peatland mining will continue to rise. Indeed, our results imply that even in the deepest reaches of the alluvial plain critical infrastructure for mining (heavy machinery, trails, and a logistical support system) is presumably already established, not only making previously difficult-to-reach peatlands more attractive to more miners, but also offering a considerably larger degree of isolation from law enforcement activity, which invariably relies on river transport. Moreover, if ever there existed any technical difficulties or cultural taboos that served to safeguard peatland in the past, these seem to have been overcome. Without a doubt, mining inside peatland is ongoing and expanding. Barring more rigorous control measures and protections, the constellation of factors points to continued mining and continued degradation of the alluvial plain, its considerable natural capital, and its peatlands, which will leave behind a long-lasting legacy of ecological, social, and economic consequences.

Data availability statement

All data that support the findings of this study are included within the article (and any supplementary files).

Acknowledgment

Funding that made field work possible was provided by: the Discovery Fund of Fort Worth, Texas, the Gordan and Betty Moore Foundation, the U.S. National Science Foundation (Grand No. 0717453) and the Programa de Ciencia y Tecnologia—FINCYT (Grant No. PIBAP-2007-005, and co-financed by the Banco International de Desarollo, BID). Staff at the Botanical Research Institute of Texas provided important institutional support during field campaigns. Javier Huinga and Angel Balerezo provided tireless assistance in the field. JEH, FW and NSM acknowledge the support of the Strategic Partner UNSAM-KIT (SPUK). AH acknowledges the following funding: Charles University (PRIMUS/23/SCI/013), Charles University Research Centre program (UNCE/24/SCI/006) and the OP JAK programme 'Natural and anthropogenic geohazards' (CZ.02.01.01/00/22_008/0004605). FW acknowledges the Deutsche Forschungsgessellschaft (DFG), Project No. 465418545.

Conflict of interest

The authors declare no conflict of interest.

ORCID iDs

Natalie Daichendt https://orcid.org/0009-0000-1089-8641
Mathias W Tobler https://orcid.org/0000-0002-8587-0560
Edgardo M Latrubesse https://orcid.org/0000-0001-5592-302X
Adam Hastie https://orcid.org/0000-0003-2098-3510
Natalia Morandeira https://orcid.org/0000-0003-3674-2981
J Ethan Householder https://orcid.org/0000-0002-5959-3504

References

Asner G P *et al* 2010 High-resolution forest carbon stocks and emissions in the Amazon *Proc. Natl Acad. Sci.* **107** 16738–42
Asner G P, Llactayo W, Tupayachi R and Luna E R 2013 Elevated rates of gold mining in the Amazon revealed through high-resolution monitoring *Proc. Natl Acad. Sci.* **110** 18454
Asner G P and Tupayachi R 2016 Accelerated losses of protected forests from gold mining in the Peruvian Amazon *Environ. Res. Lett.* **12** 094004
Bao N, Lechner A, Fletcher A, Erskine P, Mulligan D and Bai Z 2014 SPOTing long-term changes in vegetation over short-term variability *Int. J. Min. Reclam. Environ.* **28** 2–24
Boothroyd R J, Williams R D, Hoey T B, Barrett B and Prasojo O A 2021 Applications of Google Earth engine in fluvial geomorphology for detecting river channel change *WIREs Water* **8** e21496
Caballero Espejo J, Messinger M, Román-Dañobeytia F, Ascorra C, Fernandez L and Silman M 2018 Deforestation and forest degradation due to gold mining in the Peruvian Amazon: a 34-Year perspective *Remote Sens.* **10** 1903
Canty A and Ripley B 2021 Boot: bootstrap R (S-Plus) functions_. R package version 1.3–28 (available at: https://cran.r-project.org/web/packages/boot/index.html)
Csillik O and Asner G P 2020 Aboveground carbon emissions from gold mining in the Peruvian Amazon *Environ. Res. Lett.* **15** 014006
Davison A C and Hinkley D V 1997 *Bootstrap Methods and Their Application* (Cambridge University Press)
Desrochers A and van Duinen G J 2006 Peatland Fauna *Boreal Peatland Ecosystems* vol 188, ed R K Wieder and D H Vitt (Springer) pp 67–100
Dethier E N, Silman M R, Fernandez L E, Caballero Espejo J, Alqahtani S, Pauca P and Lutz D A 2023 Operation mercury: impacts of national-level armed forces intervention and anticorruption strategy on artisanal gold mining and water quality in the Peruvian Amazon *Conserv. Lett.* **16** e12978
Diringer S E, Feingold B J, Ortiz E J, Gallis J A, Araújo-Flores J M, Berky A, Pan W K Y and Hsu-Kim H 2015 River transport of mercury from artisanal and small-scale gold mining and

risks for dietary mercury exposure in Madre de Dios, Peru *Environ. Sci. Process. Impacts* **17** 478–87
Dlamini L Z D and Xulu S 2019 Monitoring mining disturbance and restoration over RBM site in South Africa using LandTrendr algorithm and Landsat data *Sustainability* **11** 6916
Draper F C, Roucoux K H, Lawson I T, Mitchard E T A, Honorio Coronado E N, Lähteenoja O, Torres Montenegro L T, Valderrama Sandoval E, Zarate R and Baker T R 2014 The distribution and amount of carbon in the largest peatland complex in Amazonia *Environ. Res. Lett.* **9** 124017
Elmes A, Yarlequé Ipanaqué J G, Rogan J, Cuba N and Bebbington A 2014 Mapping licit and illicit mining activity in the Madre de Dios region of Peru *Remote Sens. Lett.* **5** 882–91
Gilmore M P, Endress B A and Horn C M 2013 The socio-cultural importance of *Mauritia flexuosa* palm swamps (aguajales) and implications for multi-use management in two Maijuna communities of the Peruvian Amazon *J. Ethnobiol. Ethnomed.* **9** 29
Hastie A *et al* 2022 Risks to carbon storage from land-use change revealed by peat thickness maps of Peru *Nat. Geosci.* **15** 369–74
Hastie A, Householder J E, Honorio Coronado E N, Hidalgo Pizango C G, Herrera R, Lähteenoja O, de Jong J, Winton R S, Aymard Corredor G A and Reyna J 2024 A new data-driven map predicts substantial undocumented peatland areas in Amazonia *Environ. Res. Lett.* **19** 094019
Hijmans R J 2021 Raster: geographic data analysis and modeling_. R package version 3.5–2 (available at: https://CRAN.R-project.org/package=raster&gt)
Hijmans R J 2024 Terra: spatial data analysis (available at: https://CRAN.R-project.org/package=terra)
Householder J E, Janovec J P, Tobler M W, Page S and Lähteenoja O 2012 Peatlands of the Madre de Dios River of Peru: distribution, geomorphology, and habitat diversity *Wetlands* **32** 359–68
Householder J E and Page S 2022 Tropical peat swamp forests *Reference Module in Earth Systems and Environmental Sciences* (Elsevier) pp B9780128191668000000
Householder J E, Wittmann F, Janovec J P and Tobler M 2015 Montane bias in lowland Amazonian peatlands: plant assembly on heterogeneous landscapes and potential significance to palynological inference *Palaeogeogr. Palaeoclimatol. Palaeoecol.* **423** 138–48
Janovec J, Householder J E, Tobler M, Valega R, Von May R, Araujo J Z and Perez-Quijano M 2013 *Lima: WWF* (available at: https://wwf.panda.org/wwf_news/?219570/humedalesmadredediosimpactosamenazasenaguajalescochaspages244)
Joosten H 2010 The global peatland CO_2 picture: peatland status and drainage related emissions in all Countries of the world (Wetland International) p 36 available at: https://www.wetlands.org/publication/the-global-peatland-co2-picture/)
Karan S K, Samadder S R and Maiti S K 2016 Assessment of the capability of remote sensing and GIS techniques for monitoring reclamation success in coalmine degraded lands *J. Environ. Manage.* **182** 272–83
Kennedy R E and Braaten J 2020 Guide to the Google Earth engine implementation of the LandTrendr spectral-temporal segmentation algorithm (available at: https://emapr.github.io/LT-GEE/index.html)
Kennedy R E, Yang Z and Cohen W B 2010 Detecting trends in forest disturbance and recovery using yearly Landsat time series: 1. LandTrendr—temporal segmentation algorithms *Remote Sens. Environ.* **114** 2897–910
Kennedy R, Yang Z, Gorelick N, Braaten J, Cavalcante L, Cohen W and Healey S 2018 Implementation of the LandTrendr algorithm on Google Earth engine *Remote Sens.* **10** 691
Kuramoto J R 2001 Artisanal and informal mining in Peru *Mining, Minerals and Sustainable Development* p 82 (available at: https://pubs.iied.org/sites/default/files/pdfs/migrate/G00730.pdf)
Lähteenoja O, Reátegui Y R, Räsänen M, Torres D D C, Oinonen M and Page S 2012 The large Amazonian peatland carbon sink in the subsiding Pastaza-Marañón foreland basin, Peru *Glob. Change Biol.* **18** 164–78
Lasso C A, Colonnello G and Morales Rivas M 2016 *Morichales, Cananguchales y otros palmares inundables de suramerica: parte II : colombia, Venezuela, Brasil, Peru, Bolivia, Paraguay, Uruguay y Argentina* (*Serie Editorial Recursos Hidrobiologicos y Pequeros Continentales de Colombia*) (Instituto e Investigacion de Recursos Biologicos Alexander von Humbolt (IAVH)) p 573
Latrubesse E M, Cozzuol M, da Silva-caminha S A, Rigsby C A, Absy M L and Jaramillo C 2010 The Late Miocene paleogeography of the Amazon Basin and the evolution of the Amazon River system *Earth Sci. Rev.* **99** 99–124
Leifeld J and Menichetti L 2018 The underappreciated potential of peatlands in global climate change mitigation strategies *Nat. Commun.* **9** 1071
Leifeld J, Wüst-Galley C and Page S 2019 Intact and managed peatland soils as a source and sink of GHGs from 1850 to 2100 *Nat. Clim. Change* **9** 945–7
Marcus M, Hergoualc'h K, Honorio Coronado E N and Gutierrez V 2024 Spatial distribution of degradation and deforestation of palm swamp peatlands and associated carbon emissions in the Peruvian Amazon *J. Environ. Manage.* **351** 119665
Meyer D, Zeileis A and Hornik K 2006 The strucplot framework: visualizing multi-way contingency tables with vcd *J. Stat. Softw.* **17** 1–48
Mishra S, Page S E, Cobb A R, Lee J S H, Jovani-Sancho A J, Sjögersten S, Aswandi J A and Wardle D A 2021 Degradation of Southeast Asian tropical peatlands and integrated strategies for their better management and restoration *J. Appl. Ecol.* **58** 1370–87
Nicolau A P, Herndon K, Flores-Anderson A and Griffin R 2019 A spatial pattern analysis of forest loss in the Madre de Dios region, Peru *Environ. Res. Lett.* **14** 124045
Page S E, Rieley J O and Banks C J 2011 Global and regional importance of the tropical peatland carbon pool *Glob. Change Biol.* **17** 798–818
Page S E, Siegert F, Rieley J O, Boehm H D V, Jaya A and Limin S 2002 The amount of carbon released from peat and forest fires in Indonesia during 1997 *Nature* **420** 61–65
Phillips S J, Anderson R P and Schapire R E 2006 Maximum entropy modeling of species geographic distributions *Ecol. Modeling* **190** 231–59
Phillips S J, Dudik M and Schapire R E 2004 A maximum entropy approach to species distribution modeling *Proc. 21st Int. Conf. on Machine Learning* pp 655–62
Posa M R C, Wijedasa L S and Corlett R T 2011 Biodiversity and Conservation of tropical peat swamp forests *BioScience* **61** 49–57
R Core Team 2022 R: a language and environment for statistical computing *R Foundation for Statistical Computing, Vienna, Austria* (available at: https://www.R-project.org/)
R Core Team 2022 R: a language and environment for statistical computing *R Foundation for Statistical Computing* (available at: www.R-project.org/)
Räsänen M, Neller R, Salo J and Jungner H 1992 Recent and ancient fluvial deposition systems in the Amazonian foreland basin, Peru *Geol. Mag.* **129** 293–306
Rigsby C A, Hemric E M and Baker P A 2009 Late quaternary paleohydrology of the Madre de Dios River, southwestern Amazon Basin, Peru *Geomorphology* **113** 158–72
Robin X, Turck N, Hainard A, Tiberti N, Lisacek F, Sanchez J and Müller M 2011 PROC: an open-source package for R and S+ to analyze and compare ROC curves *BMC Bioinf.* **12** 1–8
Roucoux K H *et al* 2017 Threats to intact tropical peatlands and opportunities for their conservation *Conserv. Biol.* **31** 1283–92
Salo M, Hiedanpää J, Karlsson T, Cárcamo Ávila L, Kotilainen J, Jounela P and Rumrrill García R 2016 Local perspectives on

the formalization of artisanal and small-scale mining in the Madre de Dios gold fields, Peru *Extr. Ind. Soc.* **3** 1058–66
Sing T, Sander O, Beerenwinkel N and Lengauer T 2005 ROCR: visualizing classifier performance in R *Bioinformatics* **21** 3940–1
Swenson J J, Carter C E, Domec J C and Delgado C I 2011 Gold mining in the Peruvian Amazon: global Prices, deforestation, and Mercury imports *PLoS One* **6** e18875
UNEP 2022 Global Peatlands assessment—the state of the World's peatlands: evidence for action toward the conservation, restoration, and sustainable management of peatlands. summary for policy makers *Global Peatlands Initiative* (United Nations Environment Programme)
van der Hoek Y, Álvarez Solas S and Peñuela M C 2019 The palm *Mauritia flexuosa*, a keystone plant resource on multiple fronts *Biodivers. Conserv.* **28** 539–51
Wang B, Anggi Hapsari K, Horna V, Zimmermann R and Behling H 2022 Late holocene peatland palm swamp (aguajal) development, carbon deposition and environment change in the Madre de Dios region, southeastern Peru *Palaeogeogr. Palaeoclimatol. Palaeoecol.* **594** 110955
Wang B, Anggi Hapsari K, Horna V, Zimmermann R and Behling H 2023 Holocene environmental changes inferred from an oxbow lake in a Mauritia palm swamp (aguajal) in the Madre de Dios region, southeastern Peru *Rev. Palaeobot. Palynol.* **312** 104863
Wickham H 2007 Reshaping data with the reshape package *J. Stat. Softw.* **21** i12
Yard E E, Horton J, Schier J G, Caldwell K, Sanchez C, Lewis L and Gastañaga C 2012 Mercury exposure among artisanal gold miners in Madre de Dios, Peru: a cross-sectional study *J. Med. Toxicol.* **8** 441–8
Yu Z, Loisel J, Brosseau D P, Beilman D W and Hunt S J 2010 Global peatland dynamics since the last glacial maximum *Geophys. Res. Lett.* **37** L13402